

pubs.acs.org/Macromolecules Article

Substituent Effects on Ring Opening Allene Metathesis: Polymerization Rate Enhancement and Regioregularity

William J. Neary,**,** Fengyue Zhao,** Megan C. Murphy, Yu Chen, Fang Liu,* K. N. Houk,* and Jeffrey S. Moore*

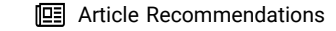


Cite This: *Macromolecules* 2024, 57, 5350–5357



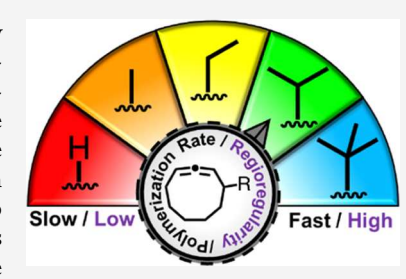
ACCESS I

Metrics & More



Supporting Information

ABSTRACT: Polyallenamers represent an emerging class of polymeric materials with highly tailorable and adaptive properties. While their generation has been achieved (via cross-coupling, postpolymerization modifications, and ring opening allene metathesis polymerization (ROAlMP)), molecular weight limitations and the inability to obtain precise microstructures have prevented the ability to utilize allenes to their full potential. Herein, we demonstrate the effects that allylic derivatization of cyclic allenes (4-*R*-1,2-CNDs) have on the polymerization rate and regioselectivity of ROAlMP. Bulky substituents were shown to favor the formation of distal products, leading to perfectly regioregular polymerizations (>97% head-to-tail). Kinetic investigations indicated that bulky substituents also led to large polymerization rate enhancements (>20×), allowing for the generation of high molecular



weight material ($M_{\rm n}$ > 120 kDa) and effective chain extension. Density functional theory calculations indicate that bulky substituents destabilize the metallacyclobutane intermediate to a greater extent than the transition state (cycloreversion), leading to unprecedented rate enhancements.

INTRODUCTION

From the storage of genetic information to the selectivity of enzymes, the regulation of the monomer sequence plays a critical role in the function of biological machinery. For example, biocatalysts carry out polymerizations at the ultimate level of precision (sequence-defined polymer), as sequence mutations or deletions can lead to genetic diseases such as cystic fibrosis and sickle cell anemia. Although much less complex, small microstructural perturbations have a similar effect on the performance of synthetic polymeric materials, leading to altered conductivities, stabilities, degradability, and thermomechanical properties. As precise control of polymers remains a challenge that obscures structure—property relationship analysis, new synthetic tools for the generation of well-defined materials are needed.

Ring opening metathesis polymerization (ROMP) presents an attractive synthetic tool for the generation of precise microstructures of variant periodicities. Upon hydrogenation of the resulting polyalkenamer, poly(ethylene- $per-\alpha$ -olefin) structures are generated, providing a model system to investigate branching length and frequency effects in polyethylene. The generation of these well-defined periodic polymers is currently accomplished through two unique strategies. First, the polymerization of symmetrical monomers can be used where the direction of monomer insertion is inconsequential to the final microstructure, leading to no microstructural defects. While this method is the most straightforward, it is limited to odd-numbered-size rings (cyclopropene, cyclopentene, cycloheptene, and norbornene) and can be challenging to

incorporate into larger systems due to remote functionalization challenges. Alternatively, the regioregular polymerization of asymmetrical monomers is amenable to all ring sizes and can be used to generate well-defined periodic polymers. In this case, the degree of regioregularity is dependent upon the steric environment at the active site and varies based on derivatization location (allylic⁷ vs vinylic⁸) and ring size.⁹ While both strategies provide access to periodic microstructures, rapid diversification of the resulting backbone is challenging due to the limited reactivity of the polyalkenamer.

In comparison, allenes represent a reactive and multidivergent functional group that has the potential for rapidly diversifying polymeric materials. ¹⁰ Although allenes have become a synthetic linchpin for organic chemists, due to challenges associated with their incorporation into polymeric materials, allenes have rarely been employed in soft materials. ¹¹ Compared to traditional polymerization methodologies of allenes that yield alternating sp^2 - sp^3 -hybridized microstructures of limited utility, successful generation of polymeric material containing allenes has been accomplished through both crosscoupling polymerization strategies ¹² and postpolymerization modifications of polyalkenamers (Scheme 1). ^{13,14} Although

Received: March 28, 2024 Revised: May 13, 2024 Accepted: May 17, 2024 Published: May 30, 2024





Scheme 1. Polyallenamer Synthesis

these methods impose limitations on either molecular weight or microstructural regularity, promising preliminary properties (helicity, 15 fluorescence, 13 degradability 16) of the resulting material have been demonstrated. Therefore, it is hypothesized that the generation of precision polyallenamers of appreciable size will lead to a new class of functionalizable materials with highly tailorable and adaptive properties.

Recently, Bielawski and Moore independently disclosed that metathesis catalysts such as Grubbs second generation catalyst (G2) transform cyclic allenes (1,2-cyclononadiene (1,2-CND)) into linear polymers through a new strategy termed ring opening allene metathesis polymerization (ROAlMP). In comparison to standard techniques, ROAIMP was shown to preserve the allenic functionality throughout polymerization, leading to well-defined polyallenamers. 18 While this methodology allows for the generation of precision allenic microstructures of variant periodicities, initial investigations indicated that catalyst instabilities and slow propagations led to molecular weight limitations (<15 kDa) faced similarly by alternative strategies. Previously, it has been observed in metathesis-based cyclopolymerizations that polymerization efficiencies, propagation rates, and catalyst stability could be drastically improved with the incorporation of bulky substituents onto the monomer due to improved cyclization efficiencies or suppression of catalyst decomposition. 19,20 While the steric effect must be overcome in typical ring opening polymerization mechanisms and is typically thought of as deleterious, the derivatization strategy and its effects in ROAIMP were unknown and therefore tested to see if increased propagation rates and increased molecular weights could be observed. We knew that if the strategy favorably increased rates, it would become a valuable tool for the generation of periodic polymers. Herein, we report the effects of alkyl and aromatic derivatization on ROAlMP propagation rates and microstructural regularity. Insights into the polymerization rate enhancements and origin of regioselectivity are provided by density functional theory (DFT) calculations.

■ RESULTS AND DISCUSSION

As prior ROMP investigations have indicated that high degrees of regioregularity are realized through vinylic and allylic derivatizations of cyclic alkenes, we began our investigation by synthesizing various alkyl and aromatic derivatives of 1,2-CND.

Vinylic derivatives, which are obtained in 3 steps from cyclooctanone (see Supporting Information for experimental details), led to poor polymerization conversion compared to the parent 1,2-CND system under identical conditions (26 vs 81%). Concomitantly, ¹³C NMR analysis indicated that polymerizations occurred in a regiorandom fashion, indicated by multiple *sp*-hybridized allenic signals (δ > 200, Figure S57). As a result, vinylic derivatives were abandoned for allylicsubstituted derivatives. Various allylic-substituted 1,2-CNDs (Me, Et, ⁱPr, ^tBu, Ph) were synthesized in moderate yields from cyclooctene in 4 steps (Scheme S1). In short, allylic bromination of cyclooctene followed by CuI-catalyzed nucleophilic substitution led to the corresponding allylicsubstituted cyclooctenes in >68% yield. Cyclic allenes (4-R-1,2-CND) were subsequently generated on gram-scale quantities following standard Doering-Laflamme conditions, leading to the isolation of the products as clear oils in moderate yields (23-58% yields). In comparison to vinylic derivatives,²¹ allylic derivatives exhibited good stabilities (>6 months) when stored at -20 °C under argon. As the introduction of an allylic-substituent generated diastereomers, diastereomeric ratios (dr) were determined by 1D-TOCSY and gas chromatography-mass spectrometry (GCMS), indicating a dr \approx 1:1 for all monomers (Table S1).

With fully characterized gram-scale quantities of 4-R-1,2-CND on hand, polymerization regioselectivities and efficiencies were investigated. As seen in Scheme 2, three different

Scheme 2. ROAIMP Microstructural Outcomes

repeat unit regioisomers are possible, depending upon the insertion preference of G2. Formation of the Dewar-Chat Duncanson adduct at a terminal carbon of the allene (1,2 or 3,2-insertion) is required to give polymerization, while formation at the center carbon of allene (2,1 or 2,3-insertion) leads to an unreactive vinylidene carbene. Distal additions in the ROMP of allylic-substituted cyclooctenes have been shown to be preferred over proximal additions due to unfavorable steric interactions between alkyl substituents and the mesityl group of the NHC ligand of G2, leading to predominantly head-to-tail (HT) products.²² As G2 was used as our catalyst of choice for ROAlMP investigations, it was hypothesized that ROAlMP of allylic derivatives would proceed through a similar origin of regioselectivity.

Polymers were prepared at a $[M]_0/[I]_0$ = 100 (see Supporting Information for experimental detail) and characterized upon isolation via ¹H NMR analysis. Tail-to-tail (TT) and head-to-head (HH) repeat unit regioisomers were identified by comparison to spectra of poly(1,2-CND) and representative small molecule analogs, respectively. Regioselectivity determinations using ¹H NMR analysis proved

ineffective because of peak overlap between the vinylic proton of the TT product (δ = 5.06) and the alkene of the HT product (Figure S69). However, sufficiently large differences in chemical shifts between HT, TT, and HH products were observed in ¹³C NMR. As a result, quantitative ¹³C NMR analysis was used for the regioselectivity determinations. Both the allenic sp-hybridized and sp²-hybridized regions in ¹³C NMR proved to be effective for regioselectivity determinations. As seen in Figure 1, three major HT peaks for poly(4-Me-1,2-

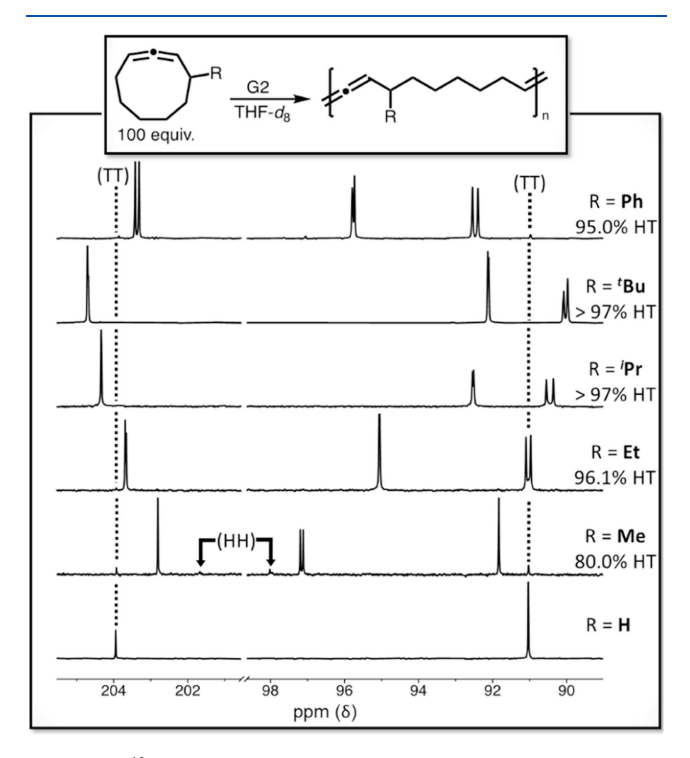


Figure 1. 13 C NMR analysis of polyallenamers (CDCl₃, 25 $^{\circ}$ C). Dashed lines indicate the TT product (poly-1,2-CND). Besides R = H, all of the major peaks represent the HT product. Long relaxation delays (D1 = 10) and integrations of similar carbons were used to calculate % HT.

CND) were observed at δ = 202.8, 97.3, and 91.8, in good agreement with literature values of 2-methylnona-3,4-diene.²³ The observation of two peaks at 97.3 (and in all other cases) is a result of polymerizing the racemic mixture of 4-Me-1,2-CND. Four minor peaks were observed at δ = 203.9, 201.7, 98.0, and 91.0, attributed to the TT (δ = 203.9 and 91.0) and HH products (δ = 201.7 and 98.0) as determined by literature precedence.²⁴ Integration of the respective peaks indicated an 80.0% preference for HT addition in poly(4-Me-1,2-CND) with minor contributions from the HH and TT repeat unit regioisomers (10.4 and 9.6%, respectively). Compared to the ROMP of 3-methylcyclooctene with G2 (93.5% HT), the alkyl substituent and the coordination site in cyclononadiene derivatives are spaced by one additional carbon, likely leading to the lower selectivity. However, as the substituent size increased to ethyl, the HT selectivity increased to 96.1%, closely matching what was previously observed for 3ethylcyclooctene (96.8% HT). Bulkier substituents such as Pr and Bu produced a perfectly regionegular material as indicated by no detectable minor peaks in ¹³C NMR. Interestingly, 4-Ph-1,2-CND (which has a larger A-value than 'Pr) only afforded 95.0% HT additions compared to >99.9%

for 3-phenylcyclooctene, highlighting the regioselectivity differences between ROMP and ROAIMP of allylic derivatives. ²⁵

Next, we decided to investigate the kinetics of these monomers in duplicate analysis via ¹H NMR, as prior investigations have shown that bulky allylic substituents drastically decrease the polymerizability of cyclic alkenes in ROMP but can accelerate propagation rates in metathesis-based cyclopolymerizations. ¹⁹ As previously demonstrated for 1,2-CND, all derivatives exhibited first-order kinetics with respect to monomer concentration (Figure 2a). ¹⁷ Large

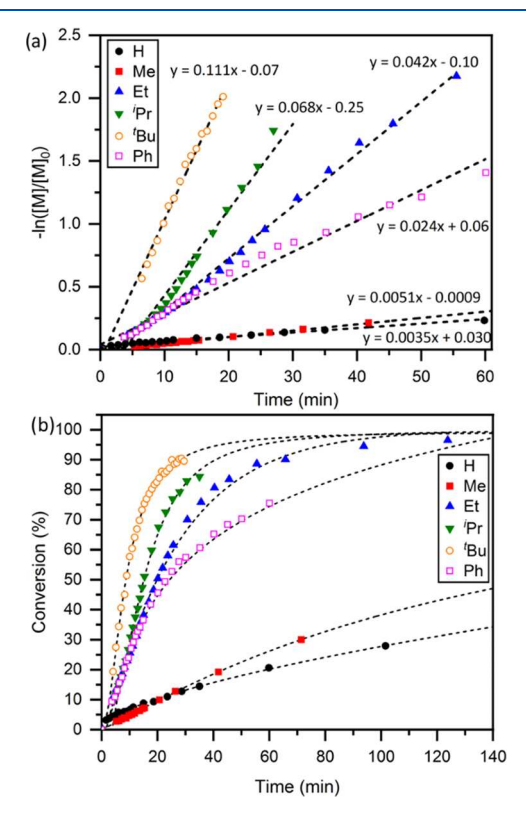


Figure 2. Kinetic analysis of 4-R-1,2-CNDs at $[M]_0/[I]_0 = 100$, $[M]_0 = 1.0$, 25 °C, THF- d_8 . (a) Linear plot of $-\ln([M]/[M]_0)$ vs time showing first-order kinetics. (b) Conversion vs time plots. The dashed lines are to help guide the eye.

differences in the polymerization rates were observed between substituents. The smallest derivative (4-Me-1,2-CND) polymerized at a similar rate ($k_{\rm obs} = 0.005 \pm 0.001 \; {\rm min}^{-1}$) as 1,2-CND ($k_{\rm obs} = 0.005 \pm 0.002 \; {\rm min}^{-1}$), reaching $\approx 25\%$ conversion after 1 h (Figure 2b). However, large rate enhancements were observed when increasing the alkyl substituent to bulkier groups. For example, the polymerization of 4-Et-1,2-CND proceeded an order of magnitude faster ($k_{\rm obs} = 0.050 \pm 0.011$ min⁻¹) than 4-Me-1,2-CND, and the bulkiest monomer (4-tBu-1,2-CND) exhibited the fastest polymerization rate $(k_{\rm obs} = 0.104 \pm 0.010 \text{ min}^{-1})$, a >20× rate enhancement in comparison to 1,2-CND. Polymer conversions of >90% for 4-^tBu-1,2-CND were realized in <30 min at a $[M]_0/[I]_0 = 100$, in stark contrast to 1,2-CND (\approx 10% conversion). It is worth noting that this trend contrasts with what has previously been observed in ROMP.²⁶ For example, 3-^tBu-cyclooctene has been shown to be nonpolymerizable due to steric effects, and 3-iPrcyclooctene polymerizes slowly (100% conversion in >24 h) in comparison to cyclooctene (100% conversion in 7 min).²⁷ We

also note that 4-Et-1,2-CND and 4-Ph-1,2-CND seem to show a decrease in polymerization rate with time, likely due to the poor catalyst stability (Figures S92 and S95). On the other hand, 4-ⁱPr-1,2-CND shows an exponential increase, potentially indicating the slow initiation nature of G2.

As polymerization of diastereomers such as *exo* and *endo*-dicyclopentadiene²⁸ and polyhydroxyalkanoates²⁹ have shown propagation rates dependent on stereochemistry, we next investigated whether a similar phenomenon would be observed in cyclic allenes. Diastereomers of 4-^tBu-1,2-CND were isolated by preparatory high-performance liquid chromatography (prep-HPLC) as confirmed by ¹³C NMR and ¹H NMR (Figures S77 and S78), and stereochemical assignments were accomplished via 2D-NOESY (Figure S79, see SI for details). Racemic 4-^tBu-1,2-CND was subsequently polymerized and monitored via GC. As seen in Figure 3, (2R, 4S) and (2S, 4R)

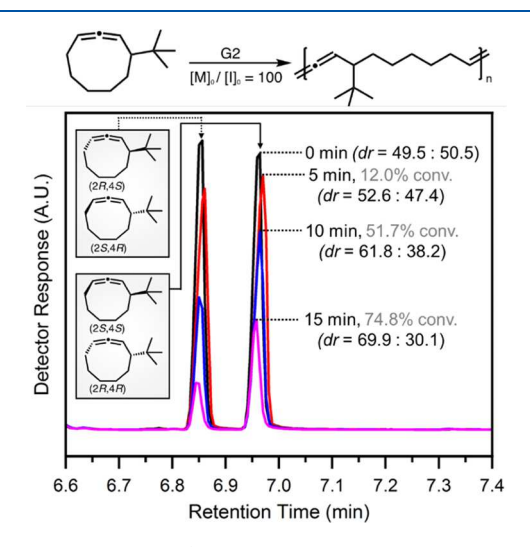


Figure 3. GC traces of 4-^tBu-1,2-CND polymerization aliquots.

were consumed $\approx 1.5 \times$ times faster ($k_{\rm obs} = 0.065 \, {\rm min}^{-1}$) than (2R, 4R) and (2S, 4S) ($k_{\rm obs} = 0.040 \, {\rm min}^{-1}$) at [M] $_0 = 1.0 \, {\rm M}$, [M] $_0/[I]_0 = 100$ (see Figure S100 for stereochemical assignment). While polymerization rate differences between diastereomers are an important contribution to the final microstructure, this rate enhancement is minimal in comparison to the effects of the size of the allylic substituent, and as a result, further investigations were not pursued.

As we had previously highlighted in our initial report, molecular weight limitations (M_p < 15 kDa) were a major challenge in ROAIMP. We next sought to investigate whether these limitations could be overcome with the use of highly reactive monomers such as 4-tBu-1,2-CND. Polymerizations at various M/I ratios (100-500) were conducted under optimized conditions, and in all cases, it led to high conversions (>65%) and an increase in molecular weight (Figures 4 and S101). These observations are in stark contrast to prior observations of 1,2-CND where, upon increasing the M/I ratios to 200, conversions plummeted to 10% with no increase of $M_{\rm n}$. Gratifyingly, $M_{\rm n} > 100$ kDa is readily obtained for poly(4- ${}^{t}Bu$ -1,2-CND) at a $[M]_{0}/[I]_{0} = 500$ with modest dispersities (D = 1.6). Except for 4-Me-1,2-CND, likely due to its slow propagation, molecular weights of >85 kDa are obtained in all other derivatives and used for thermal analysis (Table S3).

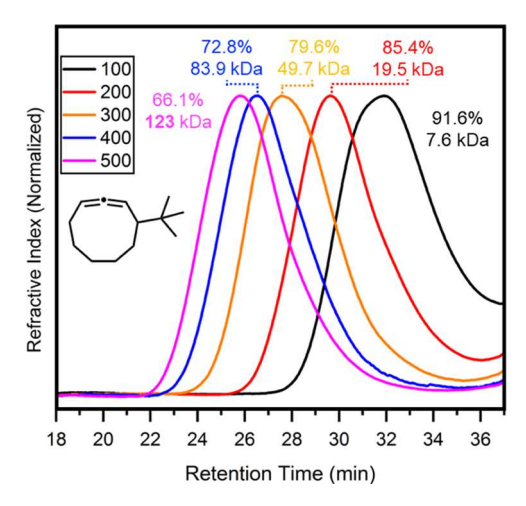


Figure 4. SEC (normalized RID vs retention time) traces of M/I trials for 4- 4 Bu-1,2-CND with respective conversion and $M_{\rm n}$ values.

While catalyst instabilities are still prevalent under these conditions (>70% residual after 90% conversion, Figure S84), we sought to investigate whether chain extension was effective for the generation of copolymers. G2 was added to 50 equiv of 4- t Bu-1,2-CND and allowed to react for 1.5 h. At this time, a small aliquot was taken for 1 H NMR and SEC analysis, and another 50 equiv of monomer was injected. After completion, M_n and conversions were obtained. As seen in Figure 5, after

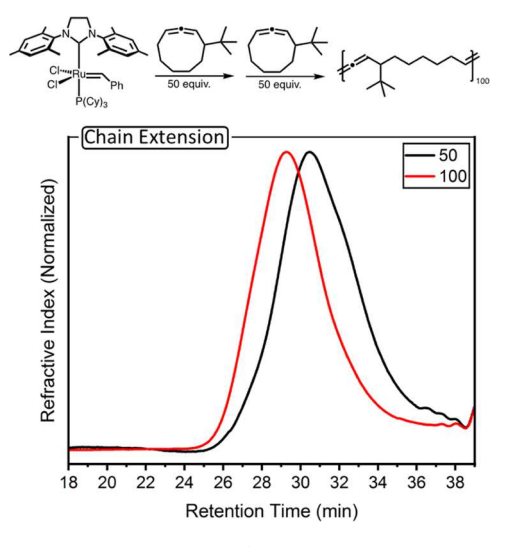


Figure 5. SEC traces (THF, 25 $^{\circ}$ C) of chain extension trials for 4- t Bu-1,2-CND.

nearly complete consumption of the monomer (96.6% conversion, $M_{\rm n}=12.2$ kDa, D=2.1 Table S2), effective chain extension to high conversion (96.3%) was obtained. The final $M_{\rm n}$ is almost perfectly double that of the first segment ($M_{\rm n}=24.5$ kDa, D=1.8). This experiment suggests that the formation of complex architectures such as block copolymers using ROAlMP is now plausible with the use of highly reactive monomers.

With the newfound ability to generate well-defined high molecular weight polyallenamers, the thermal and photophysical properties of these materials were investigated. In all cases, thermogravimetric analysis (TGA) of polyallenamers under argon showed good thermal stabilities ($T_{\rm d,onset}$ > 390 °C,

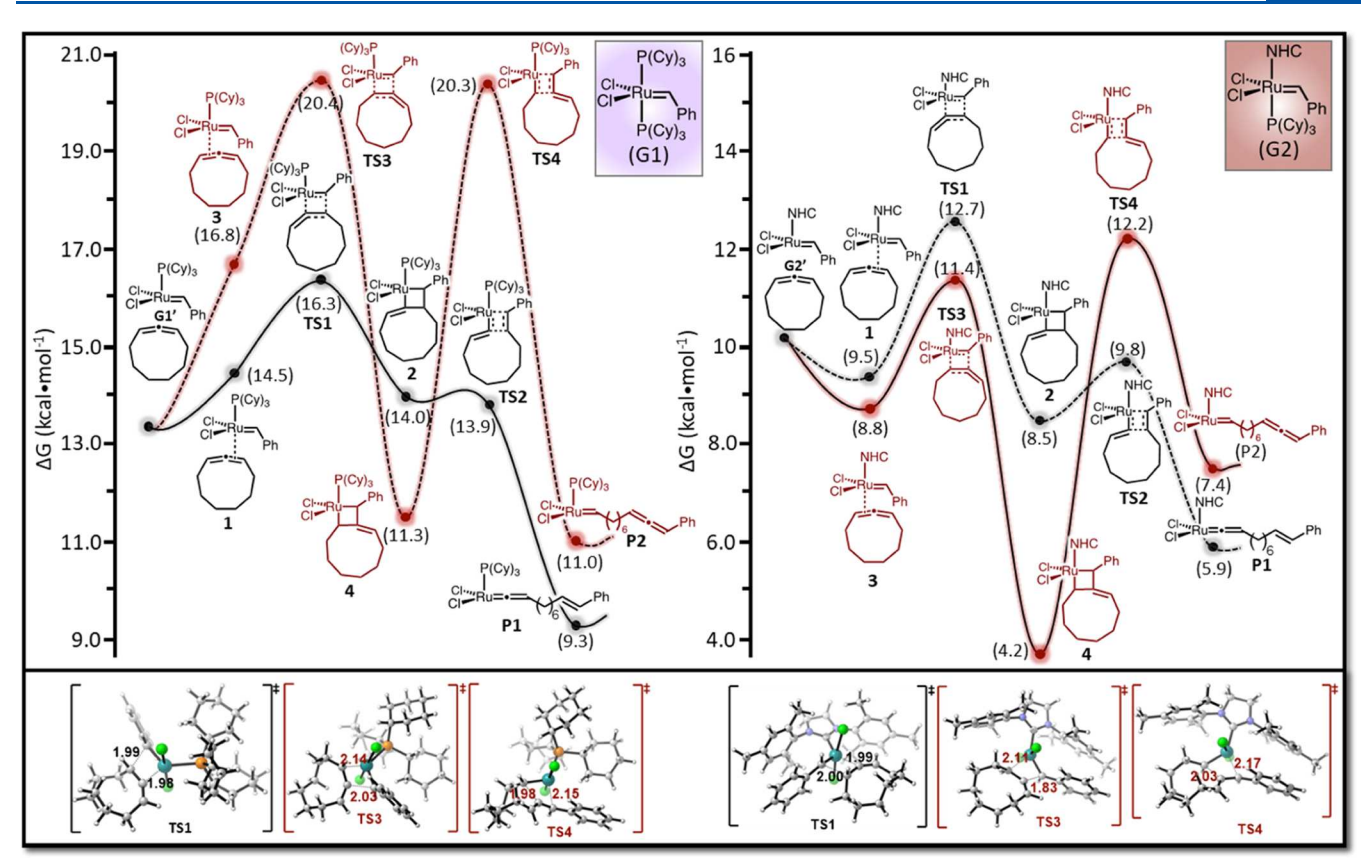


Figure 6. Gibbs free energy diagrams (in kcal·mol⁻¹) of G1- and G2-catalyzed metatheses of cyclic allenes. Solid lines indicate the preferred pathway. Red lines indicate the alkylidene formation. Black lines indicate the vinylidene formation. Bond lengths are shown in Å. Computational studies were performed with M06/6-311++G(d)-SDD(Ru) and SMD(THF)//B3LYP-D3/6-31G(d)-SDD(Ru).

Figure S96), similar to poly(1,2-CND). Differential scanning calorimetry (DSC) from -150 to $25\,^{\circ}$ C in all cases showed amorphous materials with low glass transition temperatures ($T_{\rm g} < -20\,^{\circ}$ C, Figure S97) and no observed exotherms (indicative of the lack of cross-linking events). As expected, bulkier substituents that limit the main chain flexibility led to higher $T_{\rm g}$ s. Interestingly, $T_{\rm g}$ s of these polyallenamers are similar to that of unsaturated poly(3-*R*-cyclooctenes), indicating minimal main chain flexibility difference with the addition of a single carbon and a degree of unsaturation. Photophysical properties of polyallenamers were also investigated to test the effect that substituents and regioregularity have on the fluorescence of these materials. Similar to our prior studies, broad emissions ($\lambda_{\rm EM} = 365-660$ nm) at 2.0 mg·mL $^{-1}$ in THF were observed in all cases, consistent with recently reported allene-containing polymers (Figure S99). 13,17

We also undertook a computational investigation to gain insights into this unprecedented ROAlMP rate enhancement and the origin of regioselectivity. All DFT calculations were done within the Gaussian 16^{30} program. The geometries were optimized using the B3LYP-D3³¹⁻³³ density functional with the SDD³⁴⁻³⁶ basis set for Ru and the 6-31G(d) basis set for the remaining atoms. Vibrational frequency calculations were performed at the same level of theory to confirm that the stationary point is an energy minimum or a transition state and to evaluate its zero-point vibrational energy (ZPVE) and thermal corrections at 298 K. Single-point energies were calculated at the $M06^{37}$ level with SDD basis set for Ru and 6-311++G(d,p) for the remaining atoms, and SMD³⁸ solvation

model of THF. Optimized structures are illustrated with CYLview.

Previously, we observed that the choice of catalyst dictated the mechanism between vinylidene formation (with Grubbs first generation catalyst, G1) and polymerization (with G2). To understand the origins of these selectivities, both pathways were studied for G1 and G2, and the Gibbs free energy diagrams are shown in Figure 6 for the initiation step and in Figure S102 for the propagation. G1 shows a preference for the formation of ruthenium vinylidene in initiation. The addition of ruthenium to the central carbon of allene is favored compared to the addition of it to the terminus carbon (Figure 6 left, TS1 vs TS3, $\Delta\Delta G^{\ddagger} = 4.1 \text{ kcal·mol}^{-1}$). This occurs due to the relatively electrophilic nature of the ruthenium in the alkylidene formed from G1 and its preference to attack at the central carbon of allene. In the favored vinylidene formation pathway, the formation of metallacyclobutane intermediate via TS1 is the rate-limiting step (RLS, $\Delta G^{\ddagger} = 16.3 \text{ kcal·mol}^{-1}$), and the formation of the ruthenium vinylidene was slightly more exergonic than the ruthenium alkylidene (Figure 6 left, P1 vs P2, $\Delta \Delta G = 1.7 \text{ kcal·mol}^{-1}$). For G2, a slight preference in the pathway leading to alkylidene formation was observed. In contrast to G1, the RLS is the formation of alkylidene from metallacyclobutane via TS4, similar to what has previously been observed in the ROMP of cyclooctene.²² While the minimal difference between pathways for initiation was observed for G2 (Figure 6, TS1 vs TS4, $\Delta\Delta G^{\ddagger} = 0.5$ kcal· mol-1), a study on the propagation process indicated a preference for the experimentally observed pathway (Figure \$102, $\Delta \Delta G^{\ddagger} = 2.3 \text{ kcal·mol}^{-1}$).

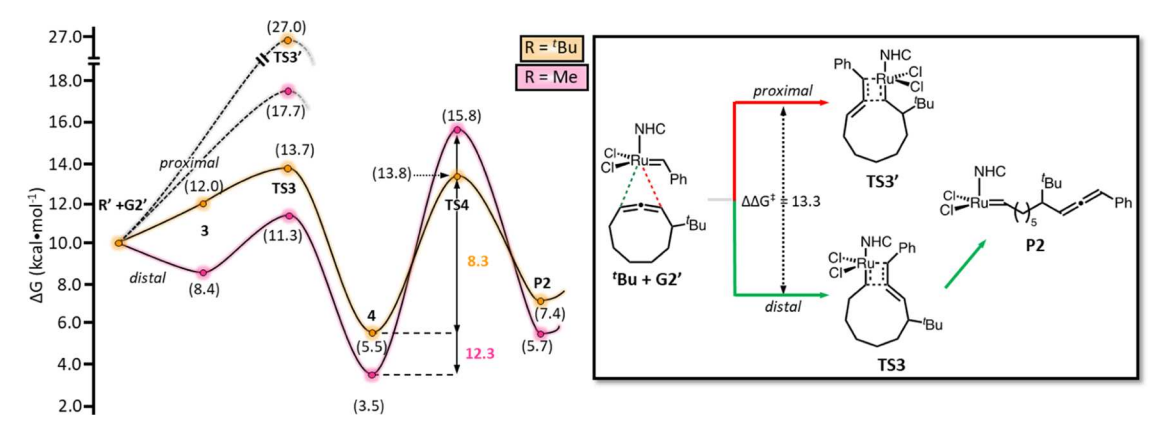


Figure 7. Gibbs free energy diagrams (in kcal·mol⁻¹) of G2-catalyzed metathesis of substituted cyclic allenes R' (R = Me and tBu). Computational studies were performed with M06/6-311++G(d)-SDD(Ru) and SMD(THF)//B3LYP-D3/6-31G(d)-SDD(Ru).

Table 1. Distortion/Interaction-Activation Strain Analysis for Intermediate 4 and Transition State TS4

	4					TS4				
	Me	Ph	Et	ⁱ Pr	^t Bu	Me	Ph	Et	ⁱ Pr	^t Bu
$E_{(G2'-dis)}$	59.3	59.3	59.4	59.0	59.4	73.9	68.7	73.2	68.7	61.4
$E_{ m (R-dis)}$	45.5	46.7	45.6	57.6	60.9	137.0	138.1	136.1	135.8	111.8
$E_{ m (dis)}$	104.8	106.0	105.0	116.6	120.3	210.9	206.8	209.3	204.5	173.2
$E_{(\mathrm{int})}$	-137.1	-138.3	-136.8	-148.1	-151.9	-232.1	-229.1	-230.3	-227.7	-197.0
$E_{(m act)}$	-32.3	32.3	-31.8	31.5	31.6	21.2	22.3	-21.0	23.2	-23.8
$G_{(act)}$	-6.7	-5.9	-5.3	-5.0	-4.7	5.6	5.2	4.9	4.3	3.6

With the mechanistic pathway for 1,2-CND and G2 now established, substituted derivatives were investigated. Both proximal (ruthenium attacking C3, which is close to the substituent) and distal (ruthenium attacking C1, which is away from the substituent) insertions were investigated for all substituents (R = Me, Et, Pr, Bu, Ph). A large preference for the insertion of ruthenium distal to the substituents was observed in all cases. The left side of Figure 7 shows the calculated Gibbs free energy profile for R = Me (pink) and R = ^tBu (orange) in proximal (dashed lines) and distal (solid lines) insertions. The regioselectivity is $>2\times$ larger for R = ${}^{t}Bu$ (27.0 vs $13.7 \text{ kcal·mol}^{-1}$) than R = Me (17.7 vs $11.3 \text{ kcal·mol}^{-1}$), in accordance with the higher regioselectivity observed experimentally for $R = {}^{t}Bu$. The Gibbs free energy profile shows that bulkier substituents stabilized TS4, leading to a lower barrier of activation of the rate-limiting step. These computational results are in accordance with the trend observed for the rate enhancements.

Distortion/interaction-activation strain 40,41 analysis on the rate-limiting step (from 4 to TS4) was carried out to gain a deeper understanding of the rate enhancement (Table 1). Distortion energies correspond to the energetic cost for the reactants to be distorted into transition state geometries. Large distortion leads to an increase in the activation energy. Interaction energies correspond to the stabilizing interactions between distorted reactants in the transition state geometry. A more negative interaction energy decreases the activation energy. For intermediates 4, the distortion energy (E(dis)) increases gradually with the increase of the size of substituent

group R, especially with 'Bu group. More significant steric hindrance leads to larger distortion energy and destabilization in the formation of the four-membered ring in metal-lacyclobutane. For transition states TS4, the steric hindrance built up in intermediate 4 is partially released, and a decrease in E(dis) as the size of the substituent increases was observed. An overlay of structures is provided in the corresponding colors in Table 1 to show the conformational changes that occur as a result of steric hindrance. Interaction energies are not affected as much as distortion energies with different substituents. Overall, a highly sterically hindered substituent, such as 'Bu, destabilizes intermediate 4 more than TS4 and therefore lowers the activation barrier for the rate-limiting step.

CONCLUSIONS

The effect of allylic derivatization with simple alkyl and aromatic substituents on the ROAlMP of 1,2-CND was investigated. Bulky substituents were shown to favor distal products leading to perfectly regioregular polymerizations (>97% HT), similar to what has been observed in the ROMP of cyclic alkenes. However, bulky substituents led to large polymerization rate enhancements (>20x compared to 1,2-CND) in direct contrast to similarly substituted cyclic alkenes. DFT calculations show that rate enhancements are caused by the destabilization of the metallacyclobutane intermediate via steric hindrance, which is subsequently released in the RLS (cycloreversion) leading to lower barriers of activation. This study highlights how simple derivatization of 1,2-cyclononadiene allows for molecular weight limitations to be

overcome and the effects they have on the microstructure of the resulting polyallenamer. These results provide design insights into the next generation of highly reactive cyclic allene monomers.

ASSOCIATED CONTENT

Supporting Information

The Supporting Information is available free of charge at https://pubs.acs.org/doi/10.1021/acs.macromol.4c00699.

Synthesis; characterization; and DFT calculations (PDF)

AUTHOR INFORMATION

Corresponding Authors

William J. Neary — Department of Chemistry, University of Illinois at Urbana—Champaign, Urbana, Illinois 61801, United States; Present Address: W.J.N.: Department of Chemistry, University of California, Riverside, Riverside, California 92521, United States; orcid.org/0000-0003-3933-1571; Email: wneary@illinois.edu

Fang Liu — College of Sciences, Nanjing Agricultural University, Nanjing 210095, China; Email: acialiu@njau.edu.cn

K. N. Houk — Department of Chemistry and Biochemistry, University of California, Los Angeles, California 90095, United States; orcid.org/0000-0002-8387-5261; Email: houk@chem.ucla.edu

Jeffrey S. Moore — Department of Chemistry and Beckman Institute for Advanced Science and Technology, University of Illinois at Urbana—Champaign, Urbana, Illinois 61801, United States; orcid.org/0000-0001-5841-6269; Email: jsmoore@illinois.edu

Authors

Fengyue Zhao – College of Sciences, Nanjing Agricultural University, Nanjing 210095, China

Megan C. Murphy — Department of Chemistry, University of Illinois at Urbana—Champaign, Urbana, Illinois 61801, United States; Present Address: M.C.M.: Materials Department, Materials Research Laboratory, and Department of Chemistry and Biochemistry, University of California, Santa Barbara, California 93106, United States; orcid.org/0000-0002-0803-8973

Yu Chen – Department of Chemistry and Shenzhen Grubbs Institute, Guangdong Provincial Key Laboratory of Catalysis, Southern University of Science and Technology, Shenzhen 518055, China

Complete contact information is available at: https://pubs.acs.org/10.1021/acs.macromol.4c00699

Author Contributions

[#]W.J.N. and F.Z. contributed equally to this paper. Quantum mechanical calculations and analysis were performed by Fengyue Zhao.

Notes

The authors declare no competing financial interest.

ACKNOWLEDGMENTS

This work was supported by the NSF Center for the Chemistry of Molecularly Optimized Networks (MONET), CHE-2116298. KNH acknowledges financial support from the National Science Foundation (CHE-2153972). TGA and DSC

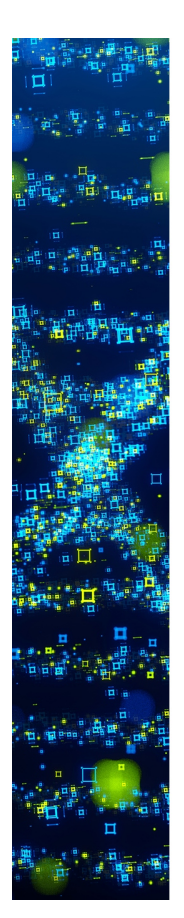
experiments were carried out in the Materials Research Laboratory Central Research Facilities, University of Illinois.

REFERENCES

- (1) Clancy, S. Genetic Mutation. Nat. Educ. 2008, 1, 187.
- (2) Jiang, X. M.; Österbacka, R.; Korovyanko, O.; An, C. P.; Horovitz, B.; Janssen, R. A. J.; Vardeny, Z. V. Spectroscopic Studies of Photoexcitations in Regioregular and Regiorandom Polythiophene Films. *Adv. Funct. Mater.* **2002**, *12*, 587–597.
- (3) Nowalk, J. A.; Swisher, J. H.; Meyer, T. Y. Consequences of isolated critical monomer sequence errors for the hydrolysis behaviors of sequenced degradable polyesters. *Polym. Chem.* **2019**, *10*, 4930–4934
- (4) Marvel, C. S.; Denoon, C. E., Jr. The Structure of Vinyl Polymers. II. I. Polyvinyl Alcohol. *J. Am. Chem. Soc.* **1938**, *60*, 1045–1051.
- (5) Zhang, J.; Matta, M. E.; Martinez, H.; Hillmyer, M. Precision Vinyl Acetate/Ethylene (VAE) Copolymers by ROMP of Acetoxy-Substituted Cyclic Alkenes. *Macromolecules* **2013**, *46*, 2535–2543.
- (6) Orski, S. V.; Kassekert, L. A.; Farrell, W. S.; Kenlaw, G. A.; Hillmyer, M. A.; Beers, K. L. Design and Characterization of Model Linear Low-Density Polyethylenes (LLDPEs) by Multidetector Size Exclusion Chromatography. *Macromolecules* **2020**, *53*, 2344–2353.
- (7) Kobayashi, S.; Pitet, L. M.; Hillmyer, M. Regio- and stereoselective ring-opening metathesis polymerization of 3-substituted cyclooctenes. *J. Am. Chem. Soc.* **2011**, *133*, 5794–5797.
- (8) Farrell, W. S.; Beers, K. L. Ring-Opening Metathesis Polymerization of Butyl-Substituted trans-Cyclooctenes. *ACS Macro Lett.* **2017**, *6*, 791–795.
- (9) Sonoda, T.; Kobayashi, S.; Tanaka, M. Periodically Functionalized Linear Polyethylene with Tertiary Amino Groups via Regioselective Ring-Opening Metathesis Polymerization. *Macromolecules* **2021**, *54*, 2862–2872.
- (10) Taylor, D. R. The Chemistry of Allenes. Chem. Rev. 1967, 67, 317–359.
- (11) Mitchell, S. M.; Niradha Sachinthani, K. A.; Pulukkody, R.; Pentzer, E. B. 100th Anniversary of Macromolecular Science Viewpoint: Polymerization of Cumulated Bonds: Isocyanates, Allenes, and Ketenes as Monomers. *ACS Macro Lett.* 2020, *9*, 1046–1059.
- (12) Hiroki, K.; Kijima, M. Synthesis and Properties of Conjugated Copolymer Having Alternate Structure of Diphenylanthracene and Allene. *Chem. Lett.* **2005**, 34, 942–943.
- (13) Galan, N. J.; Brantley, J. N. General Access to Allene-Containing Polymers Using the Skattebøl Rearrangement. *ACS Macro Lett.* **2020**, *9*, 1662–1666.
- (14) Galan, N. J.; Brantley, J. N. Precision Synthesis of Tunable Polyallenamers from "Masked" Precursors. *Macromolecules* **2023**, *56*, 305–310
- (15) Rivera-Fuentes, P.; Diederich, Francois. Allenes in Molecular Materials. *Angew. Chem., Int. Ed.* **2012**, *51*, 2818–2828.
- (16) Yu, L.; Zhou, Q.; Gao, Y.; Fu, Z.; Xiao, Y.; Li, Z.-C.; Wang, J. Synthesis of polyallenoates through copper-mediated cross-coupling of dialkynes and bis- α -diazoesters. *Chem. Commun.* **2022**, *58*, 3909–3012
- (17) Neary, W. J.; Sun, Y.; Moore, J. S. Selective Ring-Opening Allene Metathesis: Polymerization or Ruthenium Vinylidene Formation. *ACS Macro Lett.* **2021**, *10*, 642–648.
- (18) Park, G.; Bielawski, C. W. Ring Opening Metathesis Polymerization of Cyclic Allenes. *Macromolecules* **2021**, *54*, 6135–6143.
- (19) Kang, C.; Jung, K.; Ahn, S.; Choi, T.-L. Controlled Cyclopolymerization of 1,5-Hexadiynes to Give Narrow Band Gap Conjugated Polyacetylenes Containing Highly Strained Cyclobutenes. *J. Am. Chem. Soc.* **2020**, *142*, 17140–17146.
- (20) Bhaumik, A.; Peterson, G. I.; Kang, C.; Choi, T.-L. Controlled Living Cascade Polymerization to Make Fully Degradable Sugar-Based Polymers from d-Glucose and d-Galactose. *J. Am. Chem. Soc.* **2019**, *141*, 12207.

- (21) Kawase, T.Product Class 3: Cyclic Alleenes. In *Science of Synthesis*, 44, p 395, 2008, DOI: 10.1055/sos-SD-044-00311.
- (22) Martinez, H.; Miró, P.; Charbonneau, P.; Hillmyer, M. A.; Cramer, C. J. Selectivity in Ring-Opening Metathesis Polymerization of Z-Cyclooctenes Catalyzed by a Second-generation Grubbs Catalyst. ACS Catal. 2012, 2, 2547–2556.
- (23) Lavallo, V.; Frey, G. D.; Kousar, S.; Donnadieu, B.; Bertrand, G. Allene formation by gold catalyzed cross-coupling of masked carbenes and vinylidenes. *Proc. Natl. Acad. Sci. U.S.A.* **2007**, *104*, 13569–13573.
- (24) Crandall, J. K.; Batal, D. J.; Sebesta, D. P.; Lin, F. 1,4-Dioxaspiro[2.2]pentanes. Synthesis, spectroscopic properties, and reactions with nucleophiles. *J. Org. Chem.* **1991**, *56*, 1153–1166.
- (25) Solel, E.; Ruth, M.; Schreiner, P. R. London Dispersion Helps Refine Steric A-Values: Dispersion Energy Donor Scales. *J. Am. Chem. Soc.* **2021**, *143*, 20837–20848.
- (26) Beesley, R. M.; Ingold, C. K.; Thorpe, J. F. CXIX.—The formation and stability of spiro-compounds. Part I. spiro-Compounds from cyclohexane. *J. Chem. Soc., Dalton Trans.* **1915**, *107*, 1080–1106, DOI: 10.1039/CT9150701080.
- (27) Radlauer, M. R.; Matta, M. E.; Hillmyer, M. A. Regioselective cross metathesis for block and heterotelechelic polymer synthesis. *Polym. Chem.* **2016**, *7*, 6269–6278.
- (28) Rule, J. D.; Moore, J. S. ROMP Reactivity of endo- and exo-Dicyclopentadiene. *Macromolecules* **2002**, *35*, 7878–7882.
- (29) Tang, X.; Westlie, A. H.; Watson, E. M.; Chen, E. Y.-X. Stereosequenced crystalline polyhydroxyalkanoates from diastereomeric monomer mixtures. *Science* **2019**, *366*, 754–758.
- (30) Frisch, M. J.; Trucks, G. W.; Schlegel, H. B.; Scuseria, G. E.; Robb, M. A.; Cheeseman, J. R.; Scalmani, G.; Barone, V.; Petersson, G. A.; Nakatsuji, H.; Li, X.; Caricato, M.; Marenich, Av.; Bloino, J.; Janesko, B. G.; Gomperts, R.; Mennucci, B.; Hratchian, H. P.; Ortiz, Jv.; Izmaylov, A. F.; Sonnenberg, J. L.; Williams; Ding, F.; Lipparini, F.; Egidi, F.; Goings, J.; Peng, B.; Petrone, A.; Henderson, T.; Ranasinghe, D.; Zakrzewski, V. G.; Gao, J.; Rega, N.; Zheng, G.; Liang, W.; Hada, M.; Ehara, M.; Toyota, K.; Fukuda, R.; Hasegawa, J.; Ishida, M.; Nakajima, T.; Honda, Y.; Kitao, O.; Nakai, H.; Vreven, T.; Throssell, K.; Montgomery, J. A., Jr; Peralta, J. E.; Ogliaro, F.; Bearpark, M. J.; Heyd, J. J.; Brothers, E. N.; Kudin, K. N.; Staroverov, V. N.; Keith, T. A.; Kobayashi, R.; Normand, J.; Raghavachari, K.; Rendell, A. P.; Burant, J. C.; Iyengar, S. S.; Tomasi, J.; Cossi, M.; Millam, J. M.; Klene, M.; Adamo, C.; Cammi, R.; Ochterski, J. W.; Martin, R. L.; Morokuma, K.; Farkas, O.; Foresman, J. B.; Fox, D. J. Gaussian 16 Rev. C.01 Wallingford, CT, 2016.
- (31) Lee, C.; Yang, W.; Parr, R. G. Development of the Colle-Salvetti correlation-energy formula into a functional of the electron density. *Phys. Rev. B* **1988**, *37*, 785–789.
- (32) Becke, A. D. Density-functional thermochemistry. III. The role of exact exchange. *J. Chem. Phys.* **1993**, *98*, 5648–5652.
- (33) Grimme, S.; Antony, J.; Ehrlich, S.; Krieg, H. A consistent and accurate ab initio parametrization of density functional dispersion correction (DFT-D) for the 94 elements H-Pu. *J. Chem. Phys.* **2010**, 132, No. 154104.
- (34) Schwerdtfeger, P.; Dolg, M.; Schwarz, W. H. E.; Bowmaker, G. A.; Boyd, P. D. W. Relativistic effects in gold chemistry. I. Diatomic gold compounds. *J. Chem. Phys.* **1989**, *91*, 1762–1774.
- (35) Andrae, D.; Haüßermann, U.; Dolg, M.; Stoll, H.; Preuss, H. Energy-adjusted ab initio pseudopotentials for the second and third row transition elements. *Theor. Chim. Acta* **1990**, *77*, 123–141.
- (36) Dolg, M.; Wedig, U.; Stoll, H.; Preuss, H. Energy-adjusted ab initio pseudopotentials for the first row transition elements. *J. Chem. Phys.* **1987**, *86*, 866–872.
- (37) Zhao, Y.; Truhlar, D. G. The M06 suite of density functionals for main group thermochemistry, thermochemical kinetics, noncovalent interactions, excited states, and transition elements: two new functionals and systematic testing of four M06-class functionals and 12 other functionals. *Theor. Chem. Acc.* **2008**, *120*, 215–241, DOI: 10.1007/s00214-007-0310-x.
- (38) Marenich, A. V.; Cramer, C. J.; Truhlar, D. G. Universal Solvation Model Based on Solute Electron Density and on a

- Continuum Model of the Solvent Defined by the Bulk Dielectric Constant and Atomic Surface Tensions. *J. Phys. Chem. B* **2009**, *113*, 6378–6396.
- (39) Legault, C. Y. CYLview, 1.0b, Université de Sher-brooke 2009 http://www.cylview.org.
- (40) Fernández, I.; Bickelhaupt, F. M. The activation strain model and molecular orbital theory: understanding and designing chemical reactions. *Chem. Soc. Rev.* **2014**, *43*, 4953–4967.
- (41) Bickelhaupt, F. M.; Houk, K. N. Analyzing Reaction Rates with the Distortion/Interaction-Activation Strain Model. *Angew. Chem., Int. Ed.* **2017**, *56*, 10070–10086.



CAS BIOFINDER DISCOVERY PLATFORM™

STOP DIGGING THROUGH DATA —START MAKING DISCOVERIES

CAS BioFinder helps you find the right biological insights in seconds

Start your search

